

Chapter 9

Modeling and Control of PV Systems

Yongheng Yang*, **Katherine A. Kim[†]** and **Tao Ding[‡]**

*Aalborg University, Aalborg, Denmark, [†]Ulsan National Institute of Science and Technology (UNIST), Ulsan, Korean, [‡]Xi'an Jiaotong University, Xi'an, China

9.1 INTRODUCTION

Along with the fast growth in the global economy, the consumption of conventional fossil-based energy resources (e.g., coal, gas, and oil) has also been increasing. Energy consumption was high in the past due to modernization and industrialization, and it is still increasing in today's society. Because of the increased energy demand coupled with limited fossil-based energy resources, many nations are turning to sustainable energy. Many national and international strategic energy plans are being developed so that societal energy consumption can be sustainably maintained while not causing adverse impacts on the environment. Seen from this standpoint, renewable energy is very promising, and it has already gained much popularity worldwide. In 2016, the global total renewable energy capacity was more than 2000 GW [1], as shown in Fig. 9.1. It can also be seen that solar energy is the third place in terms of total capacity. At present, the two main technologies for converting the solar energy into electricity are solar photovoltaic (PV) and concentrated solar power. Between the two types, solar PV power is more often seen in today's energy conversion systems. This chapter will focus on solar PV technology and how to control its operation to fully utilize its produced power.

Abundant solar energy can be directly converted into DC electricity using semiconducting materials (e.g., crystalline Silicon), called a PV cell, which operates based on the photovoltaic effect [2]. However, the voltage level of a single PV cell is quite low (typically about 0.5 V) compared with the voltage required for many loads (e.g., batteries in an electric car, a lamp, and the electric ac grid). Hence, a number of PV cells are connected in series to increase the voltage level to construct a PV module, as illustrated in Fig. 9.2. In practice, the PV modules and panels are also connected in series to increase voltage, in parallel to increase current, or in a combination of both, which enables the powering of heavy loads

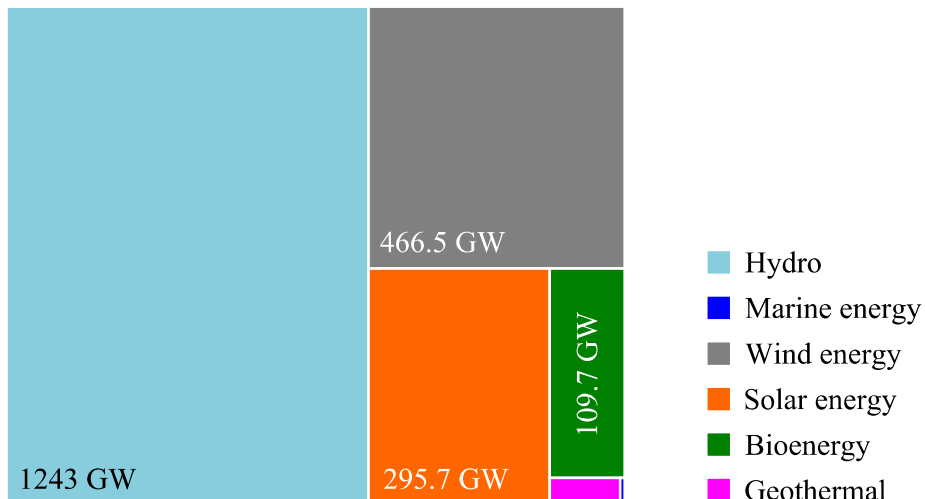


FIG. 9.1 Global renewable power capacity composition in 2016 (more than 2000 GW in total) [1], where hydro power also includes pumped storage and mixed plants; solar energy includes solar photovoltaic (290.8 GW) and concentrated solar power (4.7 GW).

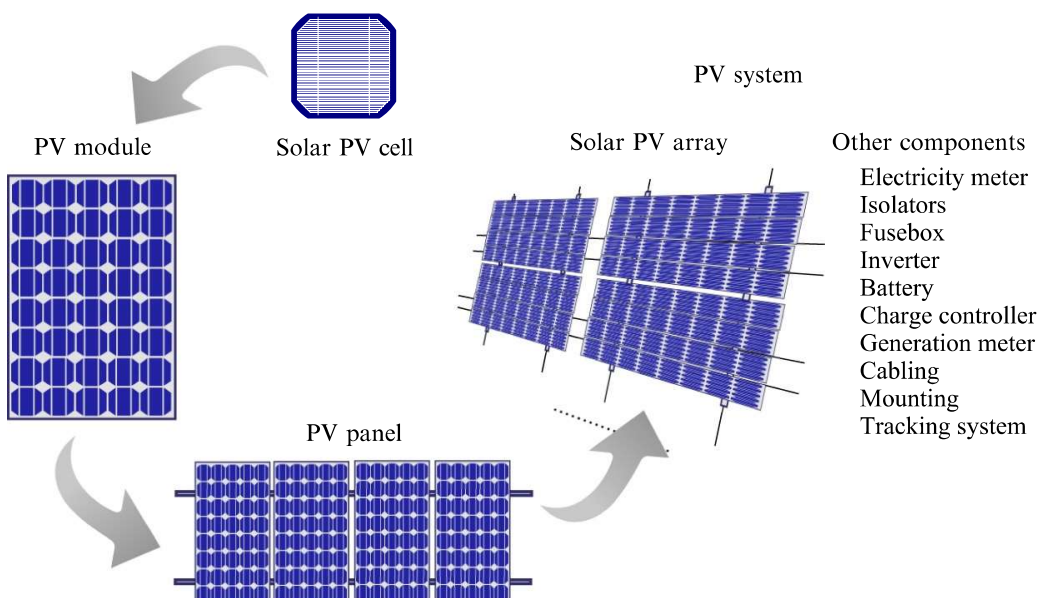


FIG. 9.2 Components of a typical PV system: from solar PV cells to a PV system. The figure is adapted from the figure published on Wikimedia. Online available: https://commons.wikimedia.org/wiki/File:From_a_solar_cell_to_a_PV_system.svg.

(high-voltage and high-power applications), as shown in Fig. 9.2. A PV system consists of, not only solar PV arrays, but many components like power converters (e.g., inverter), AC and DC isolators, and controllers.

Although the PV modules can directly power some DC loads, in most cases, power electronic converters are adopted in PV systems to improve power utilization [3]. There are two main reasons for utilizing power electronic converters: maximum power point tracking and dc-ac power conversion. PV output power is dependent on the varying environmental conditions (i.e., solar irradiance and ambient temperature), such that a maximum power point tracking (MPPT) scheme

should be employed to optimize energy capture. Additionally, for PV systems with AC loads, power electronic converters act as the link between the DC input power and the AC loads. That is, the power electronic converters are crucial to the proper operation of PV systems and control strategies for those converters should be developed to ensure the above functionalities of PV systems.

Because power electronic converters consume some power to operate properly, the efficiency of the entire PV power conversion will be affected. Topological innovations and advancements in power electronic semiconductors can contribute to an improved efficiency of PV system power converters. However, this may also complicate the overall control for the PV systems. Nevertheless, dedicated control algorithms should be investigated for power converters in PV systems to ensure efficient and reliable operation [4]. To this end, modeling is a required step to appropriately develop and evaluate control schemes.

Hence, this chapter presents the modeling of PV systems (mainly the modeling of PV modules). Commonly-used MPPT algorithms are also introduced to show how they maximize PV power production. As examples, MPPT control is implemented in both single- and double-stage PV systems based on the models of the power converters (i.e., the DC/AC inverter) described in [Chapter 6](#) of this book. Control design is demonstrated in a practical PV system example.

9.2 PV MODULE MODELING

9.2.1 PV Cell Basics—Operating Principle

PV cells, or solar cells, are semiconductor devices. In the 1950s, PV cells were initially introduced to power space satellites, but since the 1970s, they have been used in terrestrial applications as well [5,6]. Along with the continuous price drop of semiconductor materials, today, PV cells can be seen in a wide variety of applications (e.g., grid-connected systems, buildings, off-grid areas). [Fig. 9.3](#) exemplifies a roof-mounted PV system in Aalborg, Denmark, where a number of PV panels are shown and they have been connected in series or in



FIG. 9.3 Example of a roof-mounted PV system at Nordjysk Kollegium in Aalborg, Denmark.

parallel. It also shows that the surrounding environment (e.g., partial shading by trees) can negatively affect the PV power production.

PV cells can be fabricated from many different types of materials using various techniques. In terms of PV cell materials, crystalline silicon (Si) is the most commercialized. This is partially due to the high availability of low-cost silicon PV materials that has prevented new and emerging cell types from gaining significant presence in the PV market. Nevertheless, there are various emerging technologies like dye-sensitized, perovskite, organic, and quantum PV cells that have been tested in laboratories; however, initially, the efficiency is low and the cost is high [7]. Hence, intensive research is undergoing with a focus on both increasing efficiency and decreasing manufacturing cost [8]. This section will introduce the basic characteristics and operating principles of crystalline Si PV cells along with some basic considerations for designing PV systems.

A solar PV cell is actually fabricated as a large-area p-n semiconductor (e.g., Si) junction. The power generation from a PV cell is achieved by exploiting the *photovoltaic effect* that converts solar energy into electrical energy as illustrated in Fig. 9.4. The p-n junction creates a depletion region with an electric field through migration (i.e., electrons into the p-layer and holes into the n-layer), as demonstrated in Fig. 9.4. The electric field then provides a force opposing the continuous exchanging process. When a photon with sufficient energy (i.e., sunlight) hits the material, an electron will be excited by the photon and then enters into the conduction band, leaving a hole in the valence band. Due to the built-in electric field of the depletion region, the electron and hole will be swept from the junction in opposite directions. That is, holes will further concentrate toward the anode; electrons will move toward the cathode, as illustrated in Fig. 9.4, which are separated by the depletion region (the electric field). When an external path is created (e.g., the anode and cathode are connected through a bulb), the electrons will flow to “fill” the holes, and then a DC current is generated.

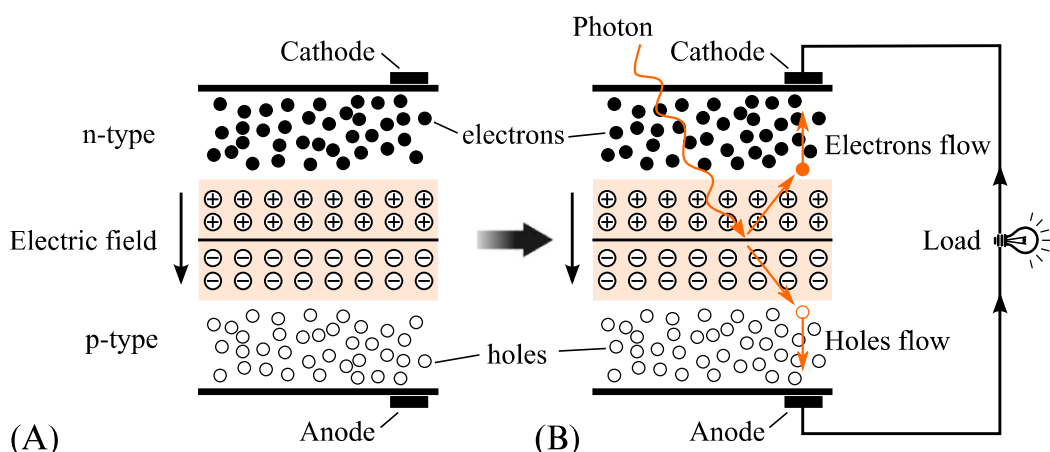


FIG. 9.4 Photovoltaic effect: (A) structure of a photovoltaic cell creating a depletion region and (B) a photon generating an electron-hole pair in a photovoltaic cell.

9.2.2 PV Cell Modeling

Based on the above discussion, the PV cell is a large area photodiode, and thus its structure of a PV cell can be modeled as various electrical components, similar to a photodiode [9–11]. Ideally, the photon-to-electron-flow process can be modeled as a current source, I_{ph} , where the generated current depends on the intensity of the sunlight hitting the cell. The p-n semiconductor junction is modeled as an ideal diode, D , as shown in Fig. 9.5. However, in practical cases, there are additional components. More specifically, the p-n junction has associated parallel capacitance, C_p , and parallel resistance, R_p . Additionally, the wire leads attached to the PV cell have some series resistance, R_s , and series inductance, L_s , as depicted in Fig. 9.5, and normally $R_p \gg R_s$. For simplicity, these parasitic components are ignored in the modeling of PV cells, but they should be reconsidered if more accurate PV models are required.

As previously discussed, the power generation from PV cells is based on the *photovoltaic effect*, where light with sufficient energy is the key to exciting electrons in the solar cell material (e.g., Si layers). This physical process is affected by many factors. That is, many environmental factors affect the characteristics of a PV cell and, thus, its power generation. There are mainly two parameters: the solar irradiance, G , and the solar cell temperature, T . Thus, the PV operating characteristics can be modeled mathematically by linking the two factors with the generated photocurrent i_{ph} , as illustrated in the following.

For simplicity, the parasitic parameters (i.e., capacitance C_p and inductance L_s) in Fig. 9.5 are ignored. Accordingly, following the Kirchhoff's Current Law (KCL), the output current of the solar PV cell i_{pv} can be obtained as

$$i_{pv} = i_{ph} - i_d - i_p \quad (9.1)$$

where i_d is the diode current and i_p is the current flowing through the parallel resistance R_p . The photocurrent is dependent of the solar irradiance level and the solar cell temperature as

$$i_{ph} = [I_{scn} + k_i(T - T_n)] \frac{G}{G_n} \quad (9.2)$$

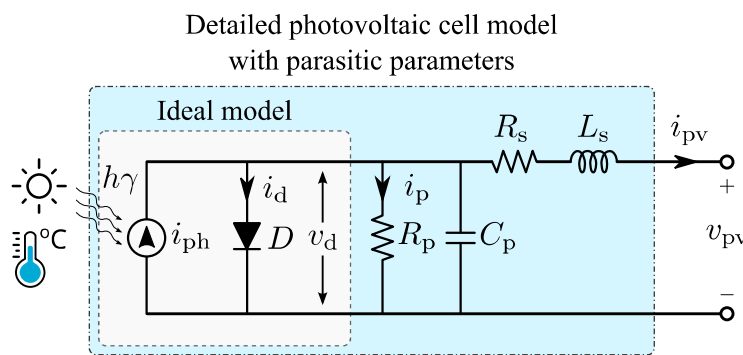


FIG. 9.5 Electrical model of a photovoltaic cell, where $h\nu$ represents photons.

with I_{scn} being the nominal short-circuit current (at the standard test condition, i.e., air mass (AM): AM1.5, cell temperature: 25°C, and solar irradiance level: 1 kW/m²), k_i being the current-temperature coefficient, G_n being the nominal solar irradiance (1 kW/m²), and T_n being the nominal cell temperature (25°C). These values can be found in the datasheets for commercial PV cells.

The diode current i_d can be expressed as an exponential function of the diode voltage as well as the solar cell temperature,

$$i_d = i_{\text{rs}} \left[\exp \left(\frac{v_d}{nk_B T/q} \right) - 1 \right] = i_{\text{rs}} \left[\exp \left(\frac{v_{\text{pv}} + i_{\text{pv}} R_s}{nk_B T/q} \right) - 1 \right] \quad (9.3)$$

where i_{rs} is the diode reverse saturation current, v_d is the diode voltage, v_{pv} is the solar cell voltage, n is the diode ideality constant (i.e., the ideality factor of the p-n junction, typically, $1 \leq n \leq 2$), k_B is the Boltzmann constant ($k_B = 1.3806503 \times 10^{-23}$ J/K), and q is the electron charge ($q = 1.60217646 \times 10^{-19}$ C). The diode saturation current i_{rs} is mainly affected by the cell temperature as

$$i_{\text{rs}} = \frac{I_{\text{scn}} + k_i(T - T_n)}{\exp \left[\frac{V_{\text{ocn}} + k_v(T - T_n)}{nk_B T/q} \right] - 1} \quad (9.4)$$

in which V_{ocn} is the nominal open-circuit voltage and k_v is the voltage-temperature coefficient.

Substituting Eq. (9.4) into Eq. (9.3), and then Eqs. (9.3) and (9.2) into Eq. (9.1), result in

$$i_{\text{pv}} = [I_{\text{scn}} + k_i(T - T_n)] \frac{G}{G_n} - \frac{I_{\text{scn}} + k_i(T - T_n)}{e^{\frac{V_{\text{ocn}} + k_v(T - T_n)}{nk_B T/q}} - 1} \cdot \left(e^{\frac{v_{\text{pv}} + i_{\text{pv}} R_s}{nk_B T/q}} - 1 \right) - \frac{v_{\text{pv}} + i_{\text{pv}} R_s}{R_p} \quad (9.5)$$

which is an equation that can be solved using the Newton-Raphson method [12]. To simplify, the ideal circuit model shown in Fig. 9.5 ($R_p = \infty \Omega$ and $R_s = 0 \Omega$) is considered. In that case, the mathematical model for a solar PV cell can be obtained as

$$i_{\text{pv}} = [I_{\text{scn}} + k_i(T - T_n)] \frac{G}{G_n} - \frac{I_{\text{scn}} + k_i(T - T_n)}{e^{\frac{V_{\text{ocn}} + k_v(T - T_n)}{nk_B T/q}} - 1} \cdot \left(e^{\frac{v_{\text{pv}}}{nk_B T/q}} - 1 \right) \quad (9.6)$$

It is implied in Eq. (9.6) that, under a given operating condition, when the PV cell output voltage is low, the PV cell will behave like a current source; conversely, when the output current is low, it will behave like a voltage source. In practice, a number of solar cells interconnected in series are encapsulated into a single, long-lasting, and stable unit, called a PV module. By taking the number of cells into account, the output current for a PV module is obtained as

$$i_{\text{pv}} = [I_{\text{scn}} + k_i(T - T_n)] \frac{G}{G_n} - \frac{I_{\text{scn}} + k_i(T - T_n)}{\frac{V_{\text{ocn}} + k_v(T - T_n)}{nk_B T N_s / q} - 1} \cdot \left(e^{\frac{V_{\text{pv}}}{nk_B T N_s / q}} - 1 \right) \quad (9.7)$$

with N_s being the number of cells in series in a PV module.

According to Eq. (9.7), the PV current can be obtained based on a given voltage. A simple solar PV model can then be implemented in MATLAB® using Simulink® Blocks or programmed models. Fig. 9.6 shows the block diagram of the solar PV model in MATLAB®, where the inputs are the solar irradiance G , the cell temperature T , and the PV module operating voltage v_{pv} , correspondingly, and the output is the PV module current i_{pv} . The mathematical model of (9.7) is programmed in C, and the audience of this book are encouraged to model the PV panels in C as an exercise. Based on the model, characteristics of a PV module can be examined.

Fig. 9.7 presents the general power-voltage (P - V) and current voltage (I - V) curves of a PV module, where the red dot indicates the maximum power point (MPP) of the P - V curve—the PV will produce the maximum power (P_{mpp}) at the MPP. Additionally, the corresponding voltage (V_{mpp}) and the current (I_{mpp}) at the MPP are also shown. It can be observed from the I - V curve in Fig. 9.7 that the PV current is relatively constant as the PV voltage changes at voltages below V_{mpp} —the PV module acts like a current source. In contrast, at voltages above V_{mpp} , the PV module voltage does not change significantly as the PV current changes—the PV module is like a voltage source—when the PV voltage is within V_{mpp} and the open circuit voltage (V_{oc}). Nevertheless, the curves in Fig. 9.7 reflect the nonlinear characteristics of PV modules. Thus, in practice, MPPT control should be applied for optimal power production, which will be discussed in Section 9.3.1. Notably, the P - V and I - V curves are for a specific

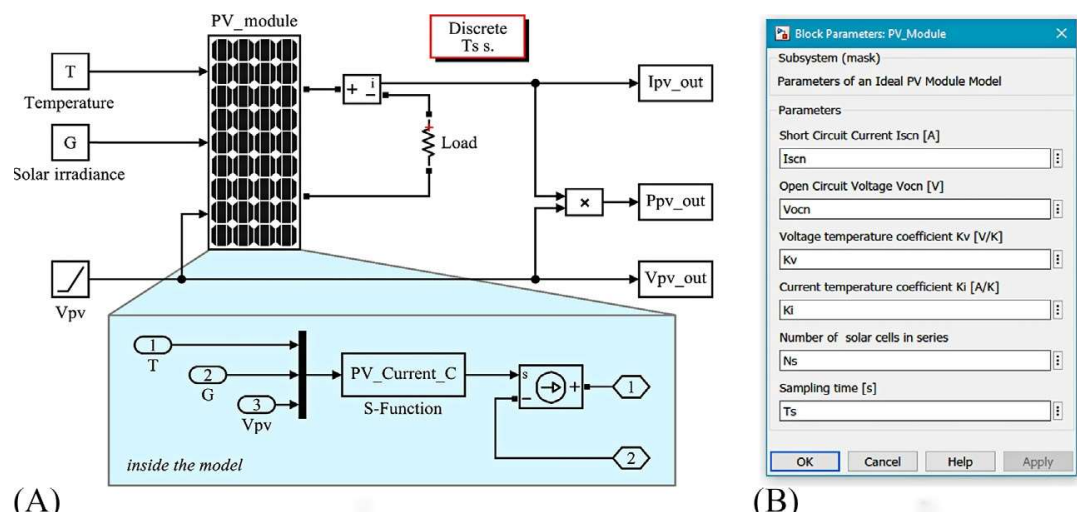


FIG. 9.6 Model of PV modules built up in MATLAB® using the user-definable block (i.e., S-Function) according to the mathematical model of (9.7): (A) Simulink® model and (B) parameter dialog box for the model. A resistor (Load) is connected.

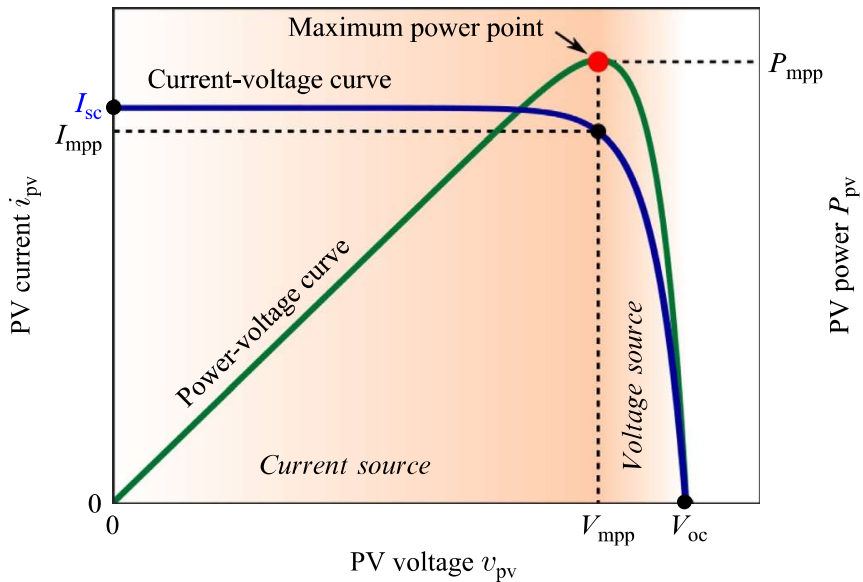


FIG. 9.7 Characteristics of PV modules (MPP: maximum power point, I_{sc} : short circuit current, V_{oc} : open circuit voltage, P_{mpp} : power at the MPP, I_{mpp} : current at the MPP, and V_{mpp} : voltage at the MPP).

condition (e.g., solar irradiance level: 1000 W/m^2 and temperature: 25°C). Over a day, both the solar irradiance level and temperature will change. Often, the changes are gradual as sunlight angles or shading patterns change such that the PV characteristics also change gradually. Sometimes quick changes can occur, e.g., due to passing clouds or birds [13], such that the curves can change drastically for just a short period of time.

As discussed previously, the solar irradiance and temperature will affect the power output from PV modules. To further investigate the impacts and also to validate the effectiveness of the model in Fig. 9.6, a commercial PV module has been investigated. Table 9.1 lists the main parameters of the PV

TABLE 9.1 Parameters of a Commercial Solar PV Module [14].

Parameter	Symbol	Value	Unit
Maximum power	P_{mpp}	65	W
Voltage at P_{mpp}	V_{mpp}	17.6	V
Current at P_{mpp}	I_{mpp}	3.69	A
Short-circuit current	I_{scn}	3.99	A
Open-circuit voltage	V_{ocn}	22.1	V
Current-temperature coefficient	k_i	0.065 ± 0.015	%/ $^\circ\text{C}$
Voltage-temperature coefficient	k_v	-80 ± 10	mV/ $^\circ\text{C}$
Number of cells	N_s	36	—

module [14], which are then programmed into the Simulink® model. Subsequently, the characteristics of the PV module under various operating conditions are obtained as shown in Fig. 9.8. It can be observed in Fig. 9.8 that the irradiance level is directly proportional to the PV current. This is in agreement with the mathematical model, where it is indicated in Eq. (9.2) that the photocurrent is proportional to the solar irradiance level. In contrast, the temperature is inversely proportional to the PV voltage. That is, as the PV cell temperature increases, the open-circuit voltage and the MPP voltage will decrease. According to these trends, a solar PV module will produce the most power when the sunlight intensity is high (i.e., the solar irradiance is strong) but the cell temperature is relatively low. However, such environmental conditions are not common in practice, since high-intensity sunlight hitting an object tends to increase its temperature at the same time. The nonlinearity of solar PV modules is also shown in Fig. 9.8.

Notably, the previously described ideal model is a relatively straightforward mathematical model. Any parasitic components are not considered. Thus, the Simulink® model may not be able to reflect the characteristics of a real PV module very accurately. For instance, in the datasheet of the adopted PV module, the power at the MPP is 65 W under standard test conditions, while the Simulink® model gives the maximum power of 70 W under the same conditions. Parasitic components in PV cells or modules, introduced and shown in Fig. 9.5, can be added to increase the model accuracy at the cost of higher model complexity. For example, if the series and shunt resistance components are considered in the model, as in Eq. (9.5), the PV characteristics become very nonlinear. In this case, much more efforts should be devoted to estimating the series and shunt resistance values according to datasheets. Further, a nonlinear solver, like the Newton-Raphson method, should be employed to solve the model numerically [9,12], as aforementioned. Nonetheless, in a similar way, a relatively accurate model for PV cells/modules can be built up in Simulink®, which is left as an exercise for the readers.

9.2.3 Configuration of PV Cells

In most PV applications, many solar PV cells are combined to produce a larger amount of power. When added together, the solar PV cells can be connected in series, parallel, or a combination of both, which form PV modules, PV panels, and PV arrays. The connection type and number of PV cells used is dependent on the voltage and current needs of the application. In most of today's PV applications, like roof-top PV installations (e.g., Fig. 9.3) and satellites, a higher voltage than a single cell is required; thus, many solar PV cells are connected in series. Typically, a standard commercial PV module is made up of 60–96 cells connected in series so that the sum at the terminals achieves an overall voltage in the range of 30–60 V.

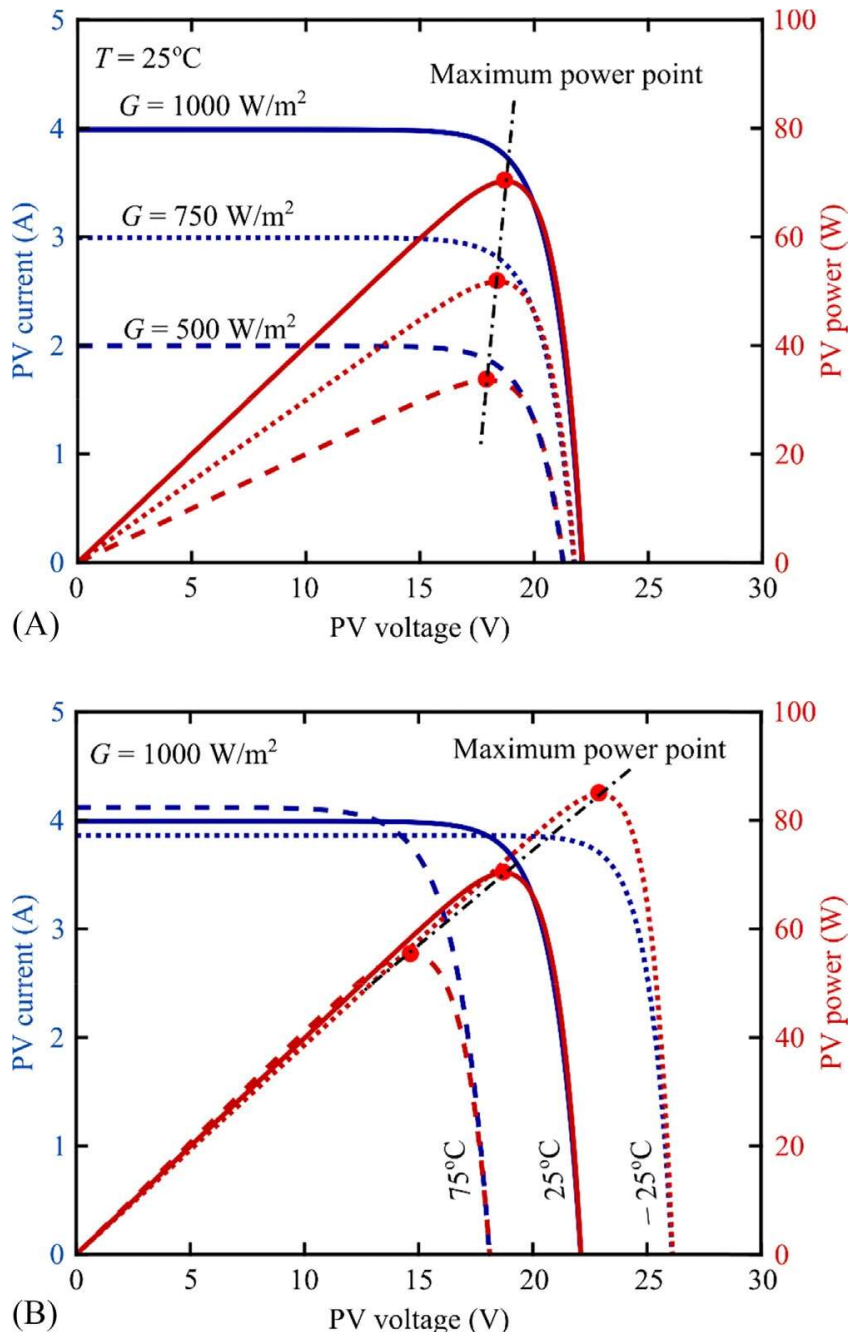


FIG. 9.8 Characteristics of a commercial PV module under different conditions: (A) fixed temperature (i.e., $T = 25^\circ\text{C}$) but varying solar irradiance level and (B) fixed solar irradiance level (i.e., $G = 1000 \text{ W/m}^2$) but varying temperature.

The physical connection structure of a PV module/panel consisting of 60 solar PV cells is shown in Fig. 9.9. To cover the area of a panel, solar cells are typically connected down one row and back up the next, as shown in Fig. 9.9. Each series connection that goes down and back up is called a substring. It can be observed that the PV module consists of three substrings with a diode that is connected across the ends of each substring. This diode is called a bypass diode [15], which allows for an additional current path around the

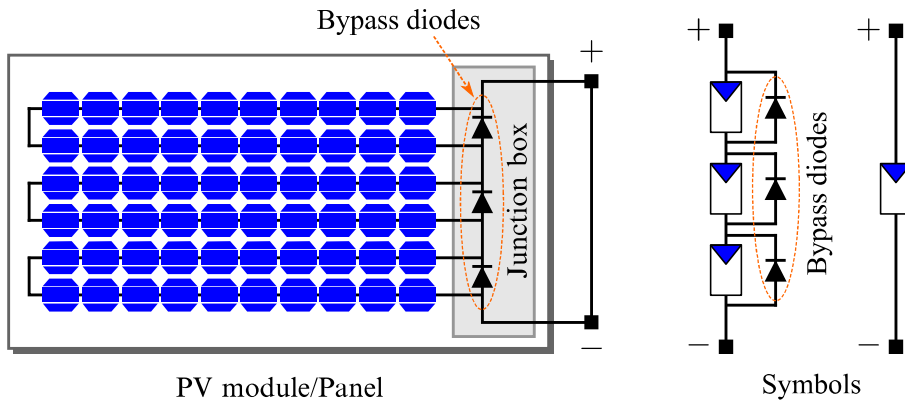


FIG. 9.9 Physical structure of a PV module consisting of 60 solar PV cells (6×10) and its electrical symbols.

substring, if solar PV cells in that substring experience a problem, such as partial shading, degradation, or a connection break in the substring. Bypass diodes help to reduce the voltage losses through the module, and the degree that these kinds of problems affect the total power production. However, various types of faults can occur in a solar PV panel that can lead to reduced power production [16].

Many PV systems are installed on rooftops or remote areas that are not easy to service if problems arise. Thus, both the panels and the associated power electronics must be able to work properly with minimal maintenance. Solar PV panels are typically rated to work continuously for 25 years or even longer, with expected degradation, generally, around 0.5%–1% per year for Si PV cells [17,18]. However, in certain conditions, PV panels tend to degrade more quickly, specifically in high heat (e.g., in the desert) or high humidity environments (e.g., tropical or seaside areas). These extreme conditions can degrade and corrode the materials that protect the cells and also degrade the PV cells themselves. Once the cells are directly exposed to the outside environment, effects of degradation occur more rapidly [19–21]. When working with PV systems, it is important that the PV cells are properly configured to meet the voltage and current needs of the application and that the cells are protected from harsh environmental conditions. Today, there are ongoing research and development efforts on fault detection and protection to improve the longevity of PV panels and the entire PV system [22–25].

9.3 CONTROL OF PV SYSTEMS

In solar PV systems, power electronic converters are normally heavily involved in transferring PV power to the loads, as illustrated in Fig. 9.10. These power electronic converters make the outputs of the power source (i.e., the PV modules) and the load compatible in terms of voltage level and frequency. For instance, in the case of grid-connected PV systems, the DC power from PV modules must be

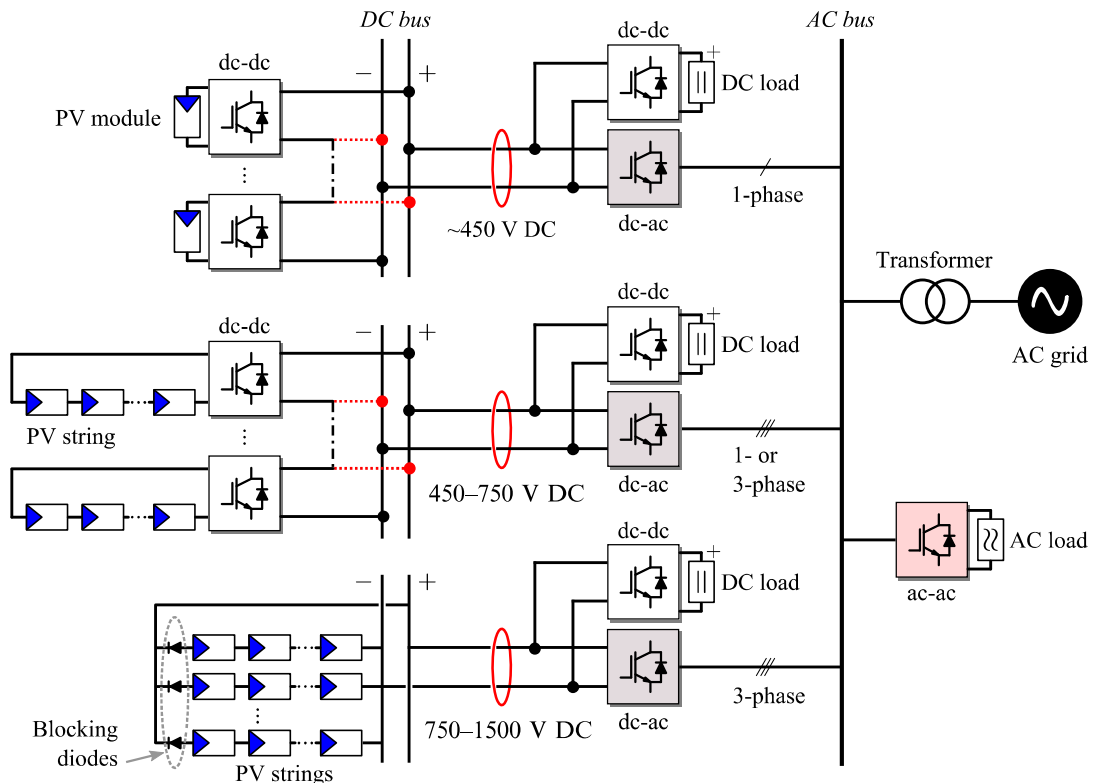


FIG. 9.10 Photovoltaic power conversion systems. As indicated, power electronic converters (e.g., DC-DC, DC-AC, and AC-AC converters) are widely used in the conversion of solar PV energy.

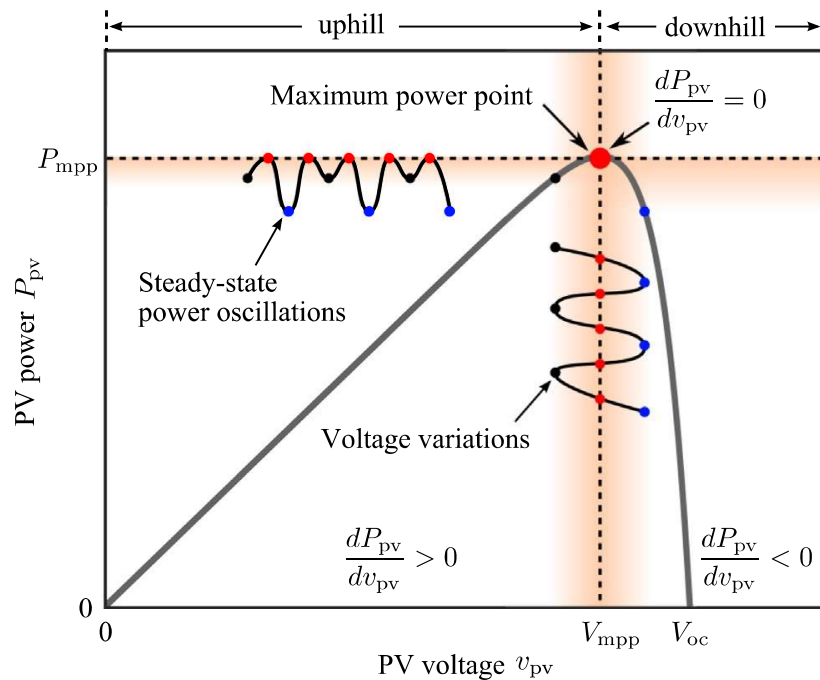
converted into AC power (e.g., 400 V, 50 Hz). Additionally, an important role of the power electronic converters is in that it enables the optimization of the PV power production even under varying environmental conditions.

9.3.1 Maximum Power Point Tracking

As discussed previously, the output power of PV modules is time variant, dependent on the solar irradiance intensity and solar cell temperature (indirectly, the ambient temperature). To maximize the power production (i.e., optimize the energy capture), MPPT control is necessary for PV systems. Hence, there have been numerous MPPT algorithms reported in the literature [26–30]. The major MPPT control algorithms are summarized in Table 9.2. Among those, the Perturb and Observe (P&O) method is the most commonly used MPPT algorithm due to its simplicity and accuracy. Actually, most of the reported MPPT control schemes are realized in accordance to the *P-V* characteristic of PV modules, as shown in Fig. 9.7, which is a hill-like curve. More specifically, on the top of the hill, the PV modules produce the maximum power, called the MPP. On the left side of the MPP, the output power has a nearly linear relationship with the PV operating voltage; while above the MPP voltage, the power drops with the increase of the PV voltage. Fig. 9.11 redepicts the general *P-V* curve of solar PV modules for illustrating the MPPT control algorithms. Ideally, the

TABLE 9.2 Pros and Cons of Major Maximum Power Point Tracking (MPPT) Methods

MPPT Methods	Advantages	Disadvantages
Perturb & Observe (P&O)/Incremental Conductance	<ul style="list-style-type: none"> ■ Simple ■ Low computation ■ Generic 	<ul style="list-style-type: none"> ■ Trade-off between speed and accuracy ■ Inaccurate under fast changing conditions
Constant Voltage (CV)	<ul style="list-style-type: none"> ■ Much simple ■ No perturbation ripple 	<ul style="list-style-type: none"> ■ Energy is wasted during V_{oc} measurement ■ Inaccuracy
Short-Current Pulse (SCP, i.e., constant current)	<ul style="list-style-type: none"> ■ Simple ■ No perturbation ripple 	<ul style="list-style-type: none"> ■ Extra switch needed for short-circuit ■ Inaccuracy
Ripple Correction Control	<ul style="list-style-type: none"> ■ Ripple amplitude offers the MPP information ■ No need for perturbation 	<ul style="list-style-type: none"> ■ Trade-off between efficiency loss due to the MPPT and due to the ripple

**FIG. 9.11** Power-voltage (P - V) characteristic of PV modules.

MPPT control should maintain the PV module operating point at the MPP to be robust and act quickly in the face of environmental variations (e.g., passing clouds inducing a sudden drop in the solar irradiance level). Those become the basic demands for the MPPT controller design.

According to Fig. 9.11, a simple P&O MPPT controller can be developed, which enables the operating point to continuously and repeatedly climb up to the top of the hill. Based on its name, the operating voltage of PV modules is perturbed (changed incrementally) in one direction first. Then, the power of the PV modules is calculated and compared with the previously-sampled value. The maximum power extraction is achieved by continuously adjusting the reference signal that is given to the controller of the power electronic converters (e.g., a boost DC-DC converter), which then adjusts the operating point of the PV module. The reference signal of the MPPT control block can be a voltage v_{pv}^* , a current i_{pv}^* , a power P_{pv}^* , or a duty cycle D^* . Taking the voltage as an example, the reference signal can be expressed as

$$v_{\text{pv}}^*(k) = v_{\text{pv}}^*(k-1) + \text{sgn}\left(\frac{\Delta P_{\text{pv}}(k)}{\Delta v_{\text{pv}}(k)}\right) \cdot v_{\text{step}} \quad (9.8)$$

where k indicates the time step, v_{step} is the perturbation step size, Δ presents the difference between the k th sampled data and the $(k-1)$ th sampled data, and $\text{sgn}(\cdot)$ is a function that determines the perturbation direction. The function $\text{sgn}(\cdot)$ is defined as

$$\text{sgn}(x) = \begin{cases} 1 & x > 0 \\ 0 & x = 0 \\ -1 & x < 0 \end{cases} \quad (9.9)$$

which reflects the operating principle of the P&O MPPT control scheme. It also indicates that the power will be oscillating around the MPP in steady state due to the repeated perturbation. The flowchart of the P&O MPPT control algorithm is shown in Fig. 9.12.

According to Fig. 9.12 and Eq. (9.8), it is known that the design of the P&O MPPT involves the selection of the step-size and the perturbation frequency (i.e., the MPPT sampling frequency). A large perturbation step-size results in fast tracking of the maximum power in response to operating condition changes. The operating point of the P&O MPPT will inevitably oscillate around the MPP, as demonstrated in Fig. 9.11. In that case, a large step-size, in return, leads to more power losses (i.e., lower accuracy), and thus low MPPT control efficiency. A rule-of-thumb for designing the step-size is to set it as around 0.1%–1% of the nominal MPP voltage V_{mpp} at STC [31]. In regard to the sampling frequency of the MPPT algorithm, in general, it should ensure that before applying the next perturbation, the entire system is already in steady-state operation. Typically, the sampling frequency can be around a few Hz and up to hundreds of Hz [26,31–34]. However, in recent studies, it has been found that the MPPT perturbation may induce interharmonics in the systems [35,36]. This may also be considered when designing the MPPT controller.

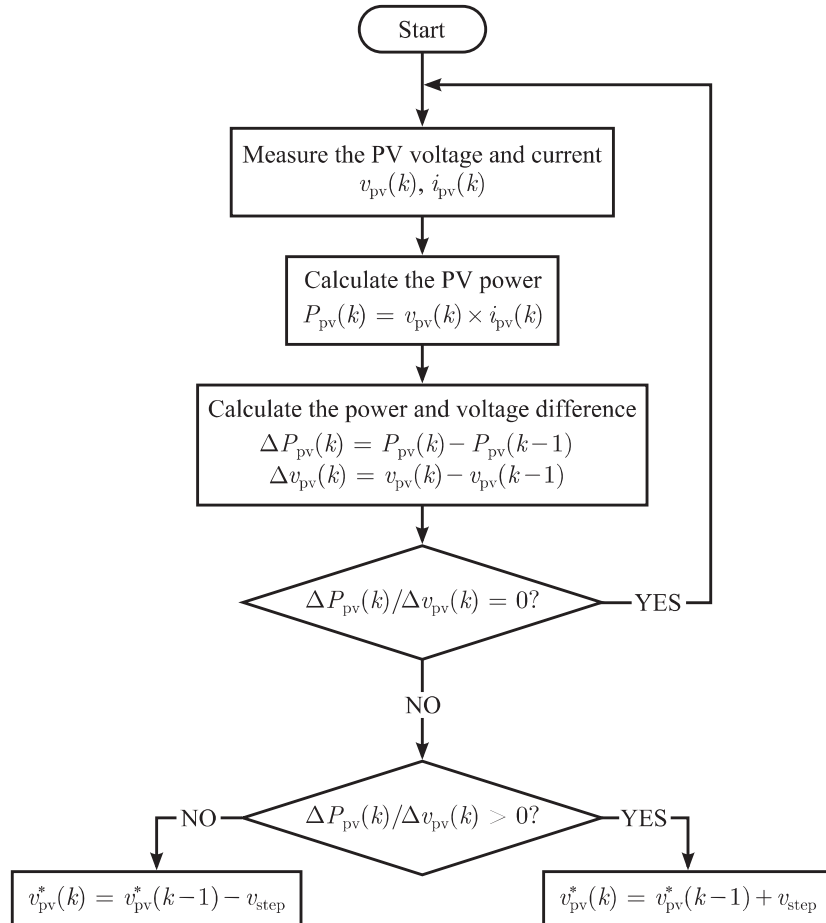


FIG. 9.12 Flowchart of the Perturb and Observe (P&O) MPPT control algorithm.

9.3.2 PV-Fed DC-DC Conversion Systems

PV modules can be connected to different loads, as demonstrated in Fig. 9.10. When powering a DC load (e.g., batteries) or a DC microgrid, DC-DC converters should be adopted either to boost the PV output voltage or to step it down, according to the load demands. In certain cases, high-voltage conversion gains are required (e.g., in microinverter applications, 30–60 V DC inputs should be converted to high DC voltages for the grid-connection to a 50-Hz 220-V AC network). PV modules employing advanced DC-DC converters (e.g., quasi-Z-source converters) are gaining more popularity in today's PV markets [3,37]. Nevertheless, the boost DC-DC converter is the most common one, which will be detailed in Section 9.4. Fig. 9.13 shows the schematic of a PV-fed DC-DC conversion system, where a resistive load is adopted.

As mentioned previously, the output of the MPPT control block can be the reference voltage, current, and power for the PV modules and also the duty cycle for the DC-DC converters. The main control objective of the DC-DC conversion systems is to optimize the power of the PV modules even under nonuniform solar irradiance and ambient temperature profiles. Normally, measuring

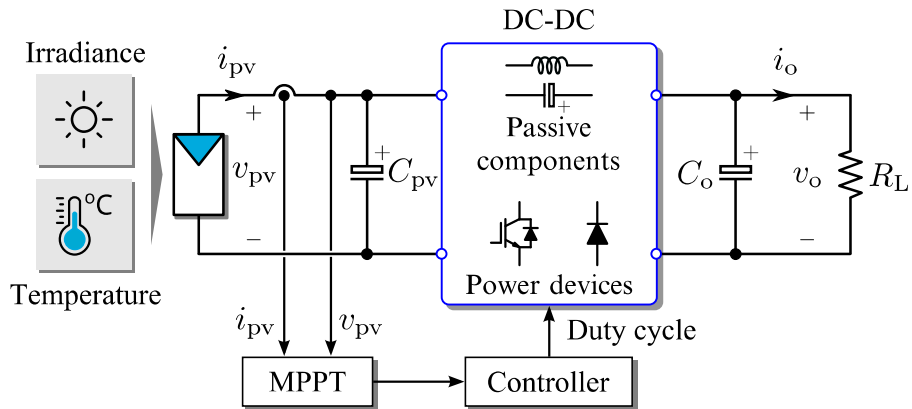


FIG. 9.13 Structure of a DC-DC conversion system fed by PV modules, where the load is a resistive load denoted as R_L . C_{PV} and C_o are the input filter and the output filter capacitor, respectively. The MPPT control algorithm shown in Fig. 9.12 can be implemented in the ‘‘MPPT’’ block in this figure.

the PV voltage and current is sufficient, while in some advanced control algorithms, other variables may be measured, which incurs more cost and complexity. Nonetheless, the criteria to select the MPPT algorithms include (1) implementation complexity, (2) tracking accuracy, and (3) robustness to fast changing conditions. For the controllers of the DC-DC converters, Chapter 3 has presented a detailed overview, and the discussed controllers (e.g., a proportional integral controller) can be employed. In addition, considering the dynamics of the PV modules, Eq. (9.7), the models of DC-DC converters (e.g., the small-signal models) together with the model of the PV modules presented in this chapter are beneficial to parameter tuning. Thus, the controller design of PV-fed DC-DC converters is not covered here; interested readers are directed to Chapter 3 of this book.

9.3.3 DC-AC Inverters for PV Systems

In many applications, voltage source converters are adopted as the interface for solar PV modules and the load (e.g., in grid-connected applications). There are mainly two ways to arrange the systems: single-stage and double-stage (i.e., DC-DC with DC-AC), as demonstrated in Fig. 9.10. For double-stage PV systems, the control is more straightforward, where the MPPT control is commonly implemented in the first stage (i.e., by controlling the DC-DC converters) and the control of the PV inverters (i.e., the DC-AC converters) is mainly to ensure proper power injection (by keeping the DC-link voltage constant). That is, the DC-link capacitor decouples the control of the DC-DC converter and the DC-AC inverter. Therefore, the MPPT control strategies can be designed according to the discussions in Section 9.3.2; while the control schemes for DC-AC converters discussed in Chapter 6 are applicable to the PV inverters.

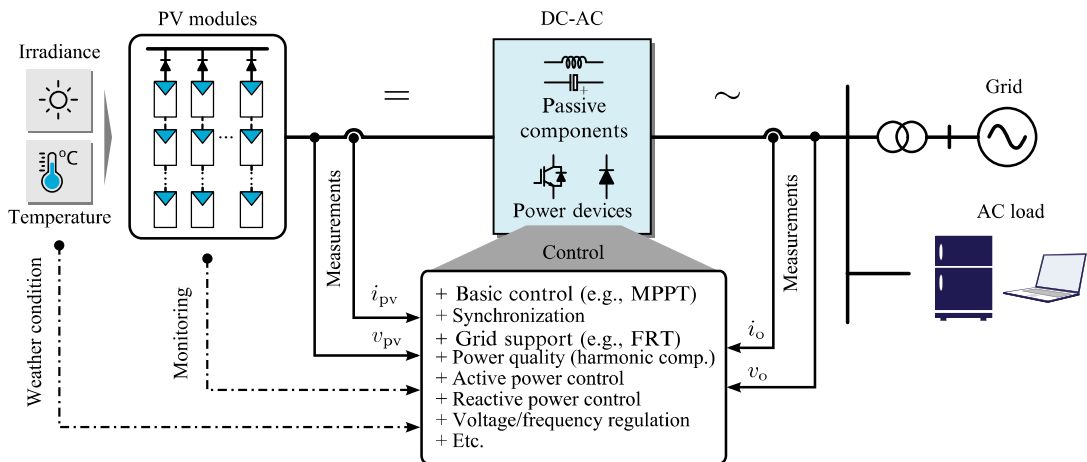


FIG. 9.14 General control structure for PV systems connected to the grid and AC loads, where the DC-AC conversion stage can also be a double-stage system (i.e., a DC-DC converter and a DC-AC converter). FRT—Fault Ride-Through.

In contrast, if a single-stage configuration is adopted, both control objectives (i.e., PV power optimization and power injection) should be accomplished in the inversion stage. Nevertheless, the major control objectives of a PV inversion system include maximum power extraction, synchronization, and power quality. There are also advanced control functionalities for PV systems, which have been illustrated in Fig. 9.14.

As shown in Fig. 9.14, the control of the PV-fed DC-AC converters is complicated in contrast to the DC-DC converters. In certain cases (e.g., the grid-connected PV systems), the entire control should be implemented at a system level and also coordinated with other controllers. For instance, in utility-scale grid-connected PV systems, it may be mandatory for PV systems to follow frequency and voltage regulations at the distribution level [38,39]. Generally, the control can be separated into two cascaded loops [4,40]: an inner current control loop and an outer loop. The outer loop is to regulate the power or the DC-link voltage, which then generates the current references for the inner control loop. Compared with the current control loop, the outer loop is slow, and a proportional or a proportional integral controller can be adopted. For the inner control loop, it should be much faster than the outer loop, and it can be implemented in different reference frames, as detailed in Chapter 6. It should be pointed out that the nonlinear hysteresis controller (also known as a bang-bang or an on-off controller) can be adopted as the inner-loop controller. The design considerations for these controllers can also be found in that chapter. In addition, the inner current should be synchronized with the AC voltage. For grid-connected systems, the synchronization can be achieved by means of phase-locked loops; while in standalone applications, an arbitrary phase may be employed depending on the load requirements. Nevertheless, details of the modeling and associated controller design of DC-AC converters can be referred to Chapter 6.

9.4 OPERATION EXAMPLES

In this section, the P&O MPPT control scheme is demonstrated first, where the PV modules are feeding power to a resistive load via a boost converter, as shown in Fig. 9.15. Three PV modules are connected in series, forming a system with the rated power of around 900 W (3×300 W). The parameters for the adopted PV module are shown in Table 9.3, where the other system parameters

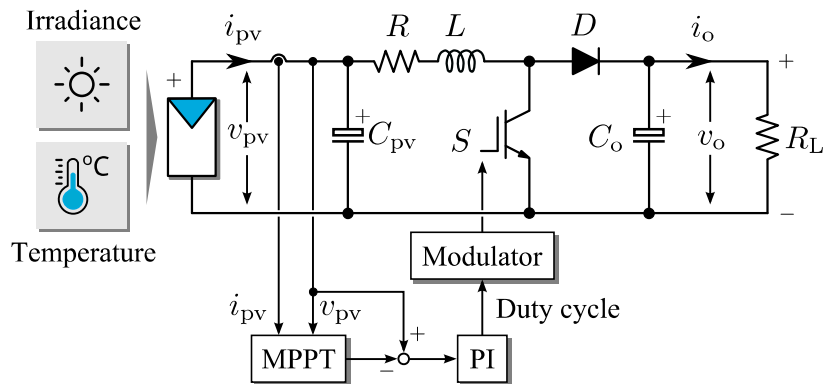


FIG. 9.15 Electrical circuit diagram of a boost conversion system fed by PV modules (PI—Proportional Integral), where the load is a resistive load R_L .

TABLE 9.3 Parameters of a PV-Fed Boost Conversion System With Three Commercial Solar PV Modules in Series [41]

Parameter	Symbol	Value	Unit
PV module			
Maximum power	P_{mpp}	300	W
Voltage at P_{mpp}	V_{mpp}	35.8	V
Current at P_{mpp}	I_{mpp}	8.37	A
Short-circuit current	I_{scn}	8.86	A
Open-circuit voltage	V_{ocn}	45.2	V
Current-temperature coefficient	k_i	0.0044	A/ $^{\circ}\text{C}$
Voltage-temperature coefficient	k_v	-0.1446	V/ $^{\circ}\text{C}$
Number of cells	N_s	72	—
Boost converter			
Boost inductor	L	1.5	mH
Resistance of the boost inductor	R	1	$\mu\Omega$
PV output capacitor	C_{pv}	220	μF
Boost output capacitor	C_o	1100	μF
Resistive load	R_L	40	Ω

are also listed. The model presented in [Section 9.2](#) is implemented (see [Fig. 9.6](#)). The switching frequency for the boost converter is $f_{sw} = 20$ kHz. A PI controller is adopted as shown in [Fig. 9.15](#), and it can be expressed as

$$G_{PI}(s) = k_p + \frac{k_i}{s} \quad (9.10)$$

with k_p and k_i being the proportional and the integral gain, respectively. The gains are designed as $k_p = 0.0025$ and $k_i = 0.58$. As stated, the P&O MPPT algorithm has been employed to track the maximum power of the PV modules, as shown in [Fig. 9.12](#). The MPPT sampling rate is 20 Hz, and the perturbation step-size is set as 0.33% of the voltage at the nominal MPP. First, the conversion system was simulated under constant conditions (solar irradiance level: 1000 W/m^2 , ambient temperature: 25°C). Then, a trapezoidal solar irradiance profile has been applied to validate the robustness of the MPPT algorithm, where the ambient temperature was fixed at 25°C . In this profile, the solar irradiance was changed from 500 to 1000 W/m^2 in 5 seconds and then experienced a fast drop to 800 W/m^2 after an operation of 8 seconds (at STC). Simulation results are shown in [Figs. 9.16 and 9.17](#).

As shown in [Fig. 9.16](#), the P&O MPPT algorithm with the designed parameters can effectively optimize the power production of the system. Furthermore,

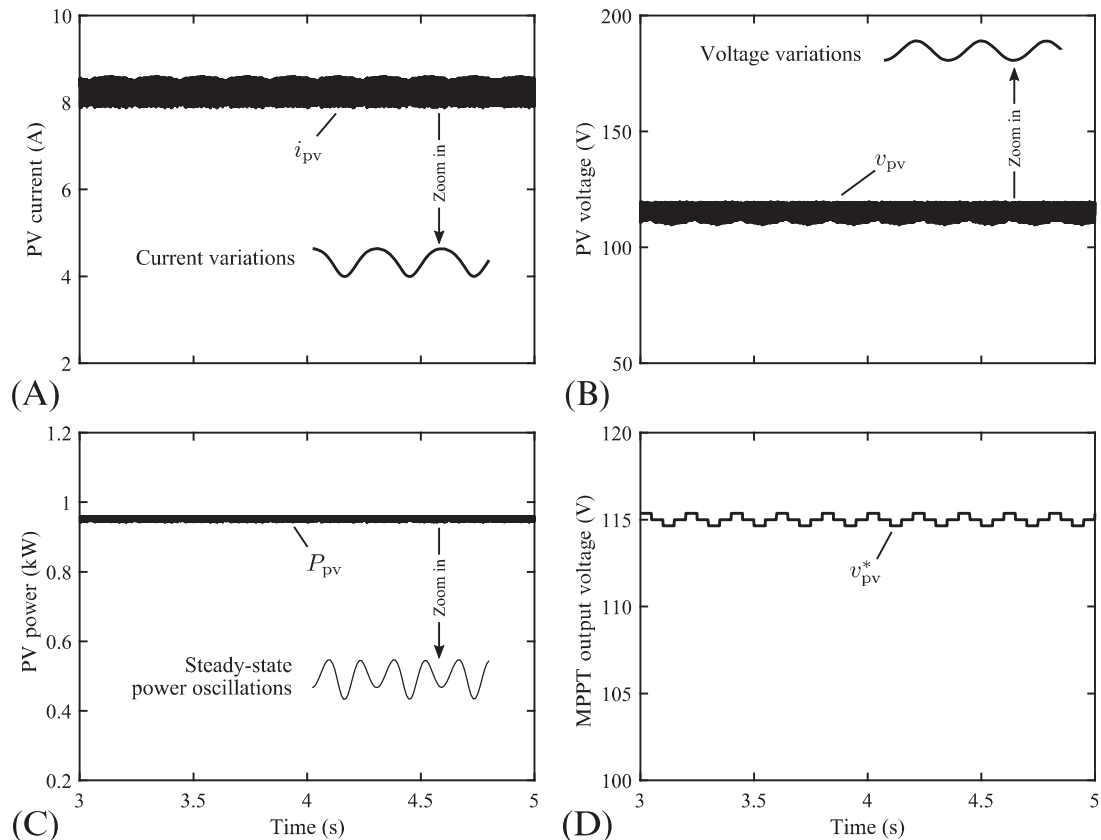


FIG. 9.16 Performance of the PV-fed boost conversion system: (A) PV current, (B) PV voltage, (C) PV power, and (D) MPPT output voltage (i.e., PV voltage reference), where the solar irradiance level is 1000 W/m^2 and the ambient temperature is 25°C .

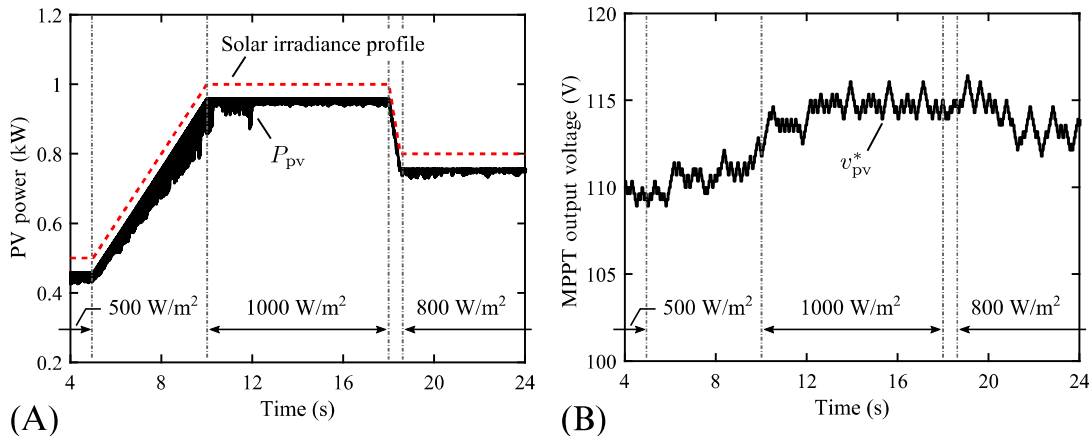


FIG. 9.17 Performance of the PV system under a trapezoidal solar irradiance profile: (A) PV power and solar irradiance profile, and (B) MPPT output voltage (i.e., PV voltage reference). In this case, the ambient temperature is constant at 25°C.

it is observed in Fig. 9.16D that the MPPT output voltage reference v_{pv}^* has three levels, which is considered as an optimal and stable operation for the MPPT controller. Additionally, this also indicates that the steady-state power will oscillate around the MPP. The resultant power losses are related to the perturbation step size. Readers are advised to explore the impact of perturbation step size on the efficiency of the MPPT control by referring to Refs. [30,31].

Following, a trapezoidal solar irradiance profile was applied to the system, as one input of the PV module model. The simulation results are shown in Fig. 9.17. As noted, under the changing solar irradiance condition the P&O MPPT algorithm may get confused, leading to loss of power production. The phenomenon has been observed in Fig. 9.17 when the solar irradiance slowly changed from 500 to 1000 W/m²—the power variations are large. This situation (i.e., the P&O algorithm gets confused) may become severe when the solar irradiance changes fast during cloudy days. In that case, advanced MPPT controllers should be developed. It should also be mentioned that the above cases are presented to show the P&O MPPT control of PV systems and to validate the modeling of PV modules in Section 9.2. More details about the parameter tuning and design are directed to Chapter 3, [26,30] in order to address the challenges under fast changing conditions.

Since many PV systems are grid-connected, a two-stage grid-connected single-phase PV system is simulated to demonstrate the basic operation and general control. Fig. 9.18 shows the hardware schematic of the exemplified system and its control structure. The PV module model presented in Section 9.2.2 has been adopted, and the entire system has been modeled in MATLAB® Simscape/Power Systems. The electrical and control parameters for the PV modules and the boost converter are the same as those for the system in Fig. 9.15, except for the PV output capacitor ($C_{\text{pv}} = 470 \mu\text{F}$). The P&O MPPT algorithm is again employed in this case study. As shown in Fig. 9.18B, the inverter is controlled

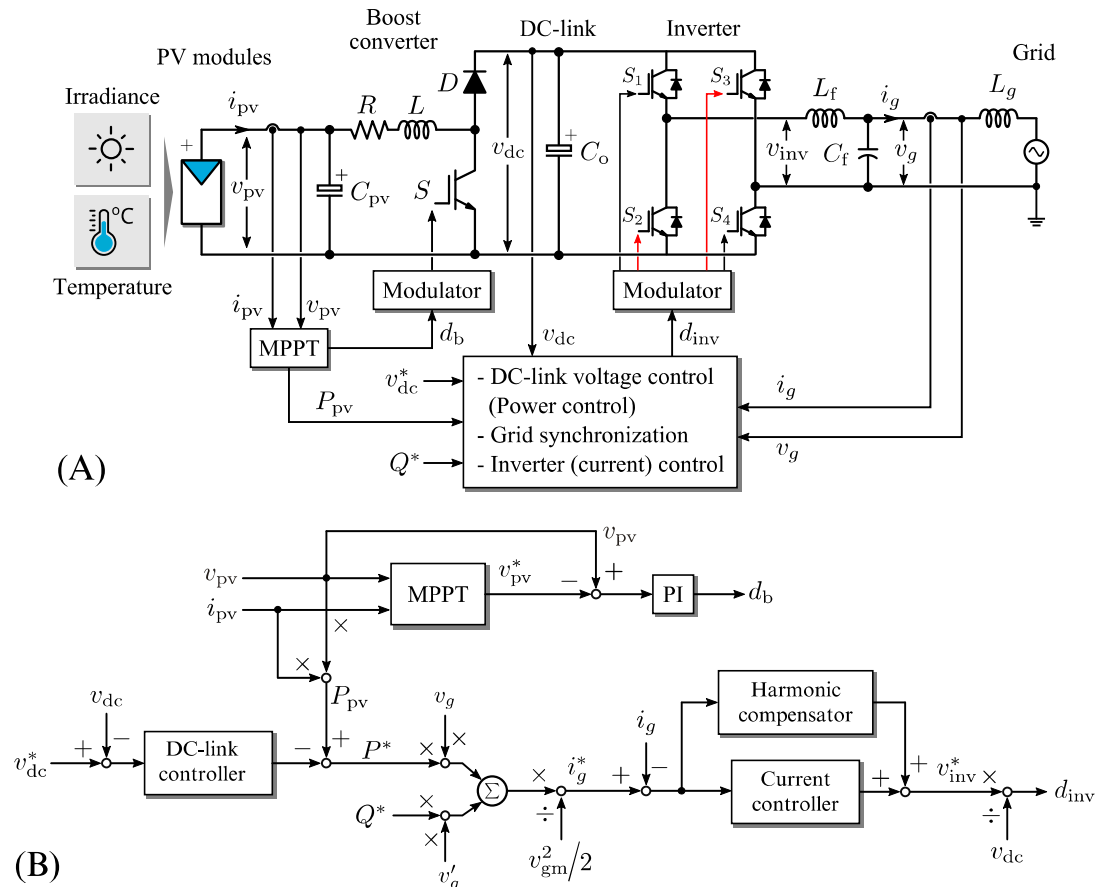


FIG. 9.18 A single-phase two-stage grid-connected PV system: (A) system hardware schematic and its general control structure and (B) detailed control block diagrams, where v_g' is the voltage in-quadrature with the grid voltage v_g , v_{gm} is the grid voltage amplitude, Q^* is the reactive power reference, and d_b , d_{inv} are the duty-cycle and modulation signal of the boost converter and the inverter respectively.

with a cascaded control system: the inner loop control regulates the grid current with a harmonic compensator, and the output loop controls the DC-link voltage and the power. A PI controller is adopted as the DC-link voltage controller $G_{PI_dc}(s)$, and a proportional resonant (PR) $G_{PR}(s)$ with multiple resonant controllers $G_{HC}(s)$ is used to regulate the injected grid current. These controllers can be expressed as

$$\begin{aligned}
 G_{PI_dc}(s) &= k_{p_dc} + \frac{k_{i_dc}}{s} \\
 G_{PR}(s) &= k_{pr} + \frac{k_{ir}s}{s^2 + \omega_0^2} \\
 G_{HC}(s) &= \frac{k_{i3}s}{s^2 + (3\omega_0)^2} + \frac{k_{i5}s}{s^2 + (5\omega_0)^2} + \frac{k_{i7}s}{s^2 + (7\omega_0)^2}
 \end{aligned} \tag{9.11}$$

where k_{p_dc} and k_{i_dc} are the proportional and integral gain of the DC-link voltage controller; k_{pr} and k_{ir} are the proportional and resonant gain of the PR current controller; k_{i3} , k_{i5} , and k_{i7} are the gains for the resonant controllers of the

harmonic compensator; and ω_0 is the grid fundamental frequency. It is clear that only the third-, fifth-, and seventh-order harmonics are compensated, as they are dominant in single-phase systems [39, 41]. The controller and the other system parameters are shown in Table 9.4. In addition, as seen in Fig. 9.18, a virtual voltage v'_g in quadrature with the grid voltage should be generated in order to calculate the current reference for the inner loop. To achieve this, a second-order generalized integrator is adopted (see Chapter 4). Simulation results are shown in Fig. 9.19, where the DC-link voltage is controlled at 450 V (i.e., $v_{dc}^* = 450$ V).

Two scenarios are simulated, where an ambient temperature of 25°C was assumed for both. In the first case, the PV system is generating the maximum power and injecting currents at unity power factor, where the solar irradiance has been decreased to 700 W/m² from 1000 W/m² at $t = t_1$. As it can be seen in Fig. 9.19A that, when there are solar irradiance changes (for instance, in practice, due to passing clouds), the entire two-stage PV system can still optimize the power production from PV modules. Additionally, the inverter is able to deliver the optimized maximum power to the grid with high-quality currents.

Furthermore, in certain applications, the PV systems may be required to provide reactive power to support the grid. Hence, the second case demonstrates the reactive power controllability of the two-stage PV system. As shown in Fig.

TABLE 9.4 Parameters of a Single-Phase Two-Stage Grid-Connected PV System

Parameter	Symbol	Value
PV inverter and grid		
Inverter output filter inductance	L_f	3.6 mH
Inverter output filter capacitor	C_f	2.35 μF
Grid voltage amplitude	v_{gm}	325 V
Grid frequency	ω_0	314 rad/s
Grid inductor	L_g	4 mH
Controllers		
DC-link PI proportional gain	$k_{p\text{-dc}}$	30
DC-link PI integral gain	$k_{i\text{-dc}}$	430
Current controller proportional gain	k_{pr}	12
Current controller resonant gain	k_{ir}	2000
Harmonic compensation resonant gains	k_{i3}, k_{i5}, k_{i7}	1400, 1200, 600

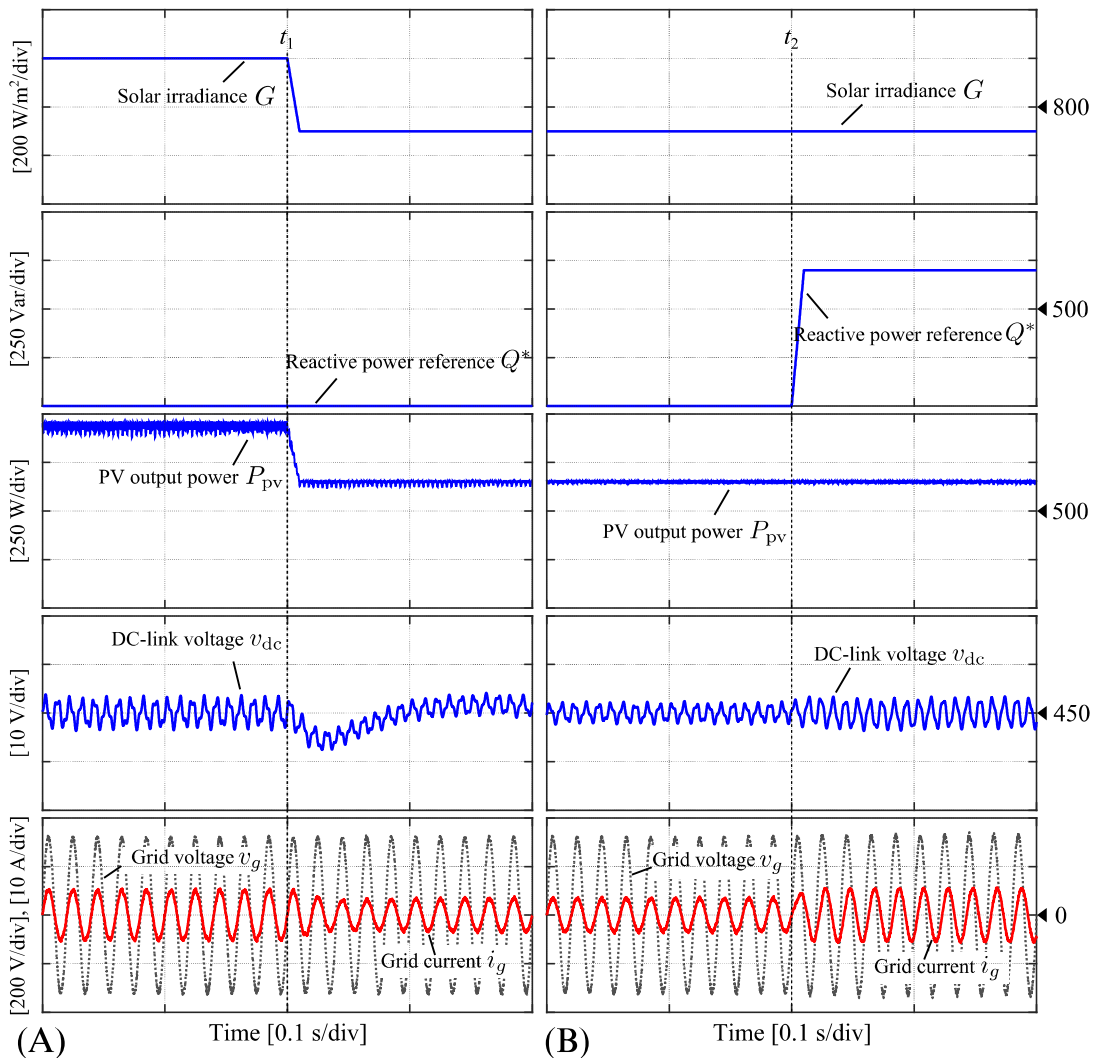


FIG. 9.19 Performance of the single-phase two-stage grid-connected PV system under various operating conditions: (A) the solar irradiance has changed to 700 W/m^2 and (B) the reactive power reference was changed to 700 Var. Ambient temperature: 25°C.

9.19B, the adopted controllers enable a proper reactive power injection to the grid upon demands. The DC-link voltage experienced minor variations during the transients, and the MPPT control of the PV modules is not affected by the control of the PV inverter. This confirms that the DC-link capacitor balances the DC power from the PV modules and the ac power injected to the grid. That is, it “decouples” the control of the entire PV system, and thus the MPPT control and the PV inverter control can be designed separately. The above examples have shown the basic operation and control of PV systems.

9.5 SUMMARY

This chapter first presented the modeling of PV systems, from a solar PV cell to a PV module, which can be configured according to the load requirements. As power electronic converters are the key to an optimal utilization of solar PV

energy, the configuration of PV power conversion systems was presented, including general controls for PV power systems. An MPPT control algorithm (i.e., the P&O MPPT algorithm) has been demonstrated on a boost DC-DC converter, with simulations under constant environmental conditions and a changing solar irradiance profile. Results have demonstrated the effectiveness of the P&O MPPT algorithm to optimize the power of PV systems and validated the PV model presented in this chapter. Notably, many efforts can be made to enhance the tracking performance of MPPT algorithms in terms of accuracy and dynamics. Additionally, a case of a two-stage single-phase grid-connected PV system was also exemplified to illustrate the basic operation and control of PV systems. The model of the PV modules was adopted and simulated to show its operation.

REFERENCES

- [1] IRENA, “Renewable Capacity Statistics 2017,” International Renewable Energy Agency (IRENA), Abu Dhabi, 2017. ISBN: 978-92-9260-018-1. Available from: http://www.irena.org/DocumentDownloads/Publications/IRENA_RE_Capacity_Statistics_2017.pdf (accessed 27.04.17).
- [2] J. Nelson, *The Physics of Solar Cells*, Imperial College Press, London, UK, 2003.
- [3] Y. Yang, F. Blaabjerg, Overview of single-phase grid-connected photovoltaic systems, *Electr. Power Compon. Syst.* 43 (12) (2015) 1352–1363.
- [4] F. Blaabjerg, R. Teodorescu, M. Liserre, A.V. Timbus, Overview of control and grid synchronization for distributed power generation systems, *IEEE Trans. Ind. Electron.* 53 (5) (2006) 1398–1409.
- [5] M.A. Green, Silicon photovoltaic modules: a brief history of the first 50 years, *Prog. Photovolt. Res. Appl.* 13 (5) (2005) 447–455.
- [6] W.T. Jewell, R. Ramakumar, The history of utility-interactive photovoltaic generation, *IEEE Trans. Energy Convers.* 3 (3) (1988) 583–588.
- [7] NREL National Center for Photovoltaics, Best Research-Cell Efficiencies for Solar PV Cells From NREL. Available from: <http://www.nrel.gov/ncpv/> (accessed 27.04.17).
- [8] M.A. Green, K. Emery, Y. Hishikawa, W. Warta, E.D. Dunlop, Solar cell efficiency tables (version 47), *Prog. Photovolt.* 24 (1) (2015) 3–11.
- [9] M.G. Villalva, J.R. Gazoli, E. Filho, Comprehensive approach to modeling and simulation of photovoltaic arrays, *IEEE Trans. Power Electron.* 24 (5) (2009) 1198–1208.
- [10] F. Spertino, J. Sumaili, H. Andrei, G. Chicco, PV module parameter characterization from the transient charge of an external capacitor, *IEEE J. Photovolt.* 3 (4) (2013) 1325–1333.
- [11] K.A. Kim, C. Xu, L. Jin, P.T. Krein, Dynamic photovoltaic model incorporating capacitive and reverse-bias characteristics, *IEEE J. Photovolt.* 3 (4) (2013) 1334–1341.
- [12] Y. Yang, K. Zhou, Photovoltaic cell modeling and MPPT control strategies, *Trans. China Electrotechn. Soc.* 26 (Sup.-1) (2011) 229–234 (in Chinese).
- [13] R.J. Serna, B.J. Pierquet, J. Santiago, R.C.N. Pilawa-Podgurski, in: Field measurements of transient effects in photovoltaic panels and its importance in the design of maximum power point trackers, *Proc. of IEEE APEC*, 2015, , pp. 3005–3010.
- [14] bp solar. “BP 365 Datasheet—65 W Photovoltaic Module,” Available from: <http://www.solarpanelstore.com/pdf/bp-365.pdf> (accessed 12.05.17).

- [15] Texas Instruments “SM74611 Datasheet—Smart Bypass Diode (Rev. B),” 2016. Available from: <http://www.ti.com/lit/ds/symlink/sm74611.pdf> (accessed 13.05.17).
- [16] K.A. Kim, P.T. Krein, Reexamination of photovoltaic hot spotting to show inadequacy of the bypass diode, *IEEE J. Photovolt.* 5 (5) (2015) 1435–1441.
- [17] A. Sangwongwanich, Y. Yang, D. Sera, F. Blaabjerg, Lifetime evaluation of grid-connected pv inverters considering panel degradation rates and installation sites, *IEEE Trans. Power Electron.* 99 (2017) 1–11.
- [18] D.C. Jordan, S.R. Kurtz, Photovoltaic degradation rates—an analytical review, *Prog. Photovolt. Res. Appl.* 21 (1) (2013) 12–29.
- [19] E.L. Meyer, E.E. van Dyk, Assessing the reliability and degradation of photovoltaic module performance parameters, *IEEE Trans. Reliab.* 53 (1) (2004) 83–92.
- [20] M. Vazquez, I. Rey-Stolle, Photovoltaic module reliability model based on field degradation studies, *Prog. Photovolt. Res. Appl.* 16 (5) (2008) 419–433.
- [21] D.C. Jordan, S.R. Kurtz, Photovoltaic degradation rates—an analytical review, *Prog. Photovolt. Res. Appl.* 21 (1) (2011) 12–29.
- [22] J. Johnson, K. Armijo, in: Parametric study of PV arc-fault generation methods and analysis of conducted DC spectrum, *Proc. of IEEE PVSC*, 2014, , pp. 3543–3548.
- [23] C.B. Jones, J.S. Stein, S. Gonzalez, B.H. King, Photovoltaic system fault detection and diagnostics using Laterally Primed Adaptive Resonance Theory neural network, *Proc. of IEEE PVSC*, 2015, pp. 1–6.
- [24] M.K. Alam, F. Khan, J. Johnson, J. Flicker, A comprehensive review of catastrophic faults in PV arrays: types, detection, and mitigation techniques, *IEEE J. Photovolt.* 5 (3) (2015) 982–997.
- [25] K.A. Kim, G.-S. Seo, B.-H. Cho, P.T. Krein, Photovoltaic hot-spot detection for solar panel substrings using AC parameter characterization, *IEEE Trans. Power Electron.* 31 (2) (2016) 1121–1130.
- [26] N. Femia, G. Petrone, G. Spagnuolo, M. Vitelli, Optimization of perturb and observe maximum power point tracking method, *IEEE Trans. Power Electron.* 20 (4) (2005) 963–973.
- [27] T. Esram, P.L. Chapman, Comparison of photovoltaic array maximum power point tracking techniques, *IEEE Trans. Energy Convers.* 22 (2) (2007) 439–449.
- [28] S. Lyden, M.E. Haque, Maximum power point tracking techniques for photovoltaic systems: a comprehensive review and comparative analysis, *Renew. Sust. Energ. Rev.* 52 (2015) 1504–1518.
- [29] E. Koutroulis, K. Kalaitzakis, N.C. Voulgaris, Development of a microcontroller-based, photovoltaic maximum power point tracking control system, *IEEE Trans. Power Electron.* 16 (1) (2001) 46–54.
- [30] D. Sera, L. Mathe, T. Kerekes, S.V. Spataru, R. Teodorescu, On the perturb-and-observe and incremental conductance MPPT methods for PV systems, *IEEE J. Photovolt.* 3 (3) (2013) 1070–1078.
- [31] H. Schmidt, B. Burger, U. Bussemas, S. Elies, How fast does an MPP tracker really need to be?, *Proc. of EU PVSEC*, 21–25 Sept., 2009, pp. 3273–3276.
- [32] N. Femia, G. Petrone, G. Spagnuolo, M. Vitelli, Optimizing sampling rate of P&O MPPT technique, *Proc. of PESC*, vol. 3, Jun. 2004, pp. 1945–1949.
- [33] M. Rosu-Hamzescu, S. Oprea, Practical guide to implementing solar panel MPPT algorithms, in: Application Note (No.: AN1521), Microchip Technology Inc, 2013.
- [34] J. Kivimaki, S. Kolesnik, M. Sitbon, T. Suntio, A. Kuperman, Revisited perturbation frequency design guideline for direct fixed-step maximum power point tracking algorithms, *IEEE Trans. Ind. Electron.* 64 (6) (2017) 4601–4609.

- [35] M. Aiello, A. Cataliotti, S. Favuzza, G. Graditi, Theoretical and experimental comparison of total harmonic distortion factors for the evaluation of harmonic and interharmonic pollution of grid-connected photovoltaic systems, *IEEE Trans. Power Delivery* 21 (3) (2006) 1390–1397.
- [36] A. Sangwongwanich, Y. Yang, D. Sera, F. Blaabjerg, in: Interharmonics from grid-connected PV systems: Mechanism and mitigation, Proc. of IFEEC—ECCE Asia, 2017, pp. 1–6.
- [37] Y. Liu, H. Abu-Rub, B. Ge, F. Blaabjerg, O. Ellabban, P.C. Loh, *Impedance Source Power Electronic Converters*, Wiley—IEEE, West Sussex, UK, 2016.
- [38] F. Blaabjerg, Y. Yang, D. Yang, X. Wang, Distributed power-generation systems and protection, *Proc. IEEE* 105 (7) (2017) 1311–1331.
- [39] Y. Yang, F. Blaabjerg, H. Wang, M.G. Simões, Power control flexibilities for grid-connected multi-functional photovoltaic inverters, *IET Renew. Power Gener.* 10 (4) (2016) 504–513.
- [40] F. Blaabjerg, D.M. Ionel (Eds.), *Renewable Energy Devices and Systems With Simulations in MATLAB® and ANSYS®*, CRC Press, Boca Raton, FL, 2017.
- [41] Yingli Green Energy Holding Co. Ltd., “YGE-U 72 Cell Series—YL300P-35b PV Module,” Product Datasheet, Available from: http://d9no22y7yqre8.cloudfront.net/assets/uploads/products/downloads/YGEU72CellSeries_US_201602_V02.pdf, (accessed 22.07.17).